npj | 2D Materials and Applications

www.nature.com/npj2dmaterials

ARTICLE OPEN

Measurements of electrically tunable refractive index of MoS_2 monolayer and its usage in optical modulators

Vasyl G. Kravets[1], Fan Wu[1,2,3], Gregory H. Auton[4], Tongcheng Yu[1], Shinji Imaizumi[1,5] and Alexander N. Grigorenko[1]

Two-dimensional materials hold a great promise for developing extremely fast, compact and inexpensive optoelectronic devices. A molybdenum disulphide (MoS_2) monolayer is an important example which shows strong, stable and gate tunable optical response even at room temperature near excitonic transitions. However, optical properties of a MoS_2monolayer are not documented well. Here, we investigate the electric field effect on optical properties of a MoS_2 monolayer and extract the dependence of MoS_2 optical constants on gating voltage. The field effect is utilised to achieve ~10% visible light modulation for a hybrid electro-optical waveguide modulator based on MoS_2. A suggested hybrid nanostructure consists of a CMOS compatible Si_3N_4 dielectric waveguide sandwiched between a thin gold film and a MoS_2 monolayer which enables a selective enhancement of polarised electro-absorption in a narrow window of angles of incidence and a narrow wavelength range near MoS_2 exciton binding energies. The possibility to modulate visible light with 2D materials and the robust nature of light modulation by MoS_2 could be useful for creation of reliable ultra-compact electro-optical hybrid visible-light modulators.

npj 2D Materials and Applications (2019)3:36 ; https://doi.org/10.1038/s41699-019-0119-1

INTRODUCTION

Two-dimensional (2D) semiconductor materials with electrically tunable optical properties could result in various applications ranging from electro-optical modulators to display screens. Indeed, it was recently established that the optical constants of 2D monolayers, in contrast to the most bulk semiconducting materials such as Si, Ge, GaAs, could vary significantly with electrical field.[1–3] As a result, 2D atomic semiconductor crystals emerged as a potential alternative to bulk semiconductors for optoelectronic applications compatible with CMOS technology.[4–6] The most investigated 2D semiconductor—a molybdenum disulphide (MoS_2) monolayer—deserves special attention as it hosts a high quality electronic system with a unique band structure and a technologically favourable band gap.[7–9] A MoS_2 monolayer is a direct band semiconductor with $E_g \approx 1.9$ eV and is composed of hexagonal planes of S and Mo atoms glued together by ionic-covalent interactions in a trigonal prismatic arrangement.[10] A unique feature of the electronic structure of MoS_2 monolayers is the significant tunability of their carrier density,[11] which is important for optoelectronic applications.[12,13] In addition, a MoS_2 monolayer is chemically and electrically stable when compared to other 2D materials.

Light absorption in a monolayer MoS_2 is produced by dipole transitions between localised *d* orbitals, which yields an absorption for a single layer MoS_2 flake at the level of 2–5% in the visible range. This is already a large value for a single layer of a 2D material since MoS_2 thickness is only ~0.65 nm. Another important contribution to MoS_2 absorption comes from excitonic excitations which are responsible for an increase in the absorption value by 5–10%.[7,10] This excitonic absorption is larger than the broadband absorption of graphene.[14] Despite the fact that the optical absorption of MoS_2 monolayers in the visible range is relatively large compared to other 2D materials,[15] its absolute value is still rather small. Therefore, in order to utilise MoS_2 monolayers in optical devices it is essential to create light trapping nanostructures which would significantly enhance light interaction with the 2D semiconductor atomic layer. The light trapping can be realised using different methods. In our previous work,[16,17] we suggested and studied hybrid plasmon-waveguide nanostructures which are capable of trapping light and enhancing absorption in 2D layers. It was recently demonstrated that enhancement of absorption from 2D monolayers can be also achieved by coupling to planar nanocavities.[18,19] Another strategy to realise resonant light trapping in single crystal 2D monolayers is based on plasmonic active layers[20] or Fabry–Perot resonators.[21]

Here, we study hybrid nanostructures that combine an atomic semiconductor with a plasmonic-metal-dielectric waveguide. We focus on a non-silicon CMOS-compatible insulating layer based on silicon nitride (Si_3N_4). Silicon nitride is a promising dielectric material because of its low linear loss, CMOS-compatibility, material stability and the ability to engineer favourable optical dispersion.[22] We investigate a simple heterostructure that optically couples light to an atomically thin semiconducting monolayer and strongly enhances the absorption of MoS_2 making possible an efficient 2D semiconductor light modulator. We demonstrate that the light absorption of a MoS_2 monolayer integrated with a Si_3N_4 waveguide can lead to a significant enhancement of visible-light polarisation-dependent modulation (~10%) in a narrow range of wavelengths near the excitonic bands ($\Delta\lambda \sim 150$ nm) and at large angles of incidence. The suggested planar metal-dielectric-2D

[1]School of Physics and Astronomy, The University of Manchester, Manchester M13 9PL, UK; [2]Key Laboratory for Non-Equilibrium Synthesis and Modulation of Condensed Matter (Ministry of Education), School of Science, Xi'an Jiaotong University, 710049 Xi'an, Shaanxi, China; [3]School of Textile Science and Engineering, Xi'an Polytechnic University, 710048 Xi'an, Shaanxi, China; [4]National Graphene Institute, University of Manchester, Manchester M13 9PL, UK and [5]Fundamental Technology Research and Development Division 2 R&D Center Sony Corporation, Atsugi Tec. 4-14-1 Asahi-cho, Atsugi 243-0014, Japan
Correspondence: Vasyl G. Kravets (vasyl.kravets@manchester.ac.uk)

Received: 17 March 2019 Accepted: 13 August 2019
Published online: 20 September 2019

semiconductor nanostructures could provide a simple and cost-effective solution for optoelectronic applications in visible light.

RESULTS

Sample preparation and characterisation

Figure 1 shows the geometry and images of the studied samples. To fabricate hybrid nanostructures covered by a MoS_2 monolayer, we have used a dry-transfer technique described in detail in Supplementary Information (SI). First, a 3 nm-thick Cr adhesion layer and a 65 nm Au film were deposited on the top of a 1 mm-thick quartz substrate using electron beam evaporation. A Si_3N_4 dielectric layer was grown by chemical vapour deposition (CVD) to cover the Au film. Then, a CVD MoS_2 monolayer (supplied by 2D Semiconductors) was transferred onto a poly(methyl-methacrylate) membrane (PMMA). The MoS_2–PMMA heterostructure was loaded into a micromanipulator and placed face-down onto a chosen Quartz/Au/Si_3N_4 sandwich after which the PMMA was dissolved producing the final device. The schematic of the device and principle of ellipsometric measurements is shown in Fig. 1a. The optical modes of a similar nanostructure were discussed in detail in our previous work.[23]

The MoS_2 monolayer thickness was first identified by the atomic force microscopy (AFM) measurement with additional verification of thickness by Raman and photoluminescence spectroscopy. AFM analysis is performed in the tapping mode on the sample to examine the surface morphology in a scan area of $17 \times 5.0\ \mu m^2$. AFM image of the nanostructure is shown in Fig. 1d. The average thickness from three scans was estimated as 0.7 nm. AFM microscopy of the device confirms monolayer nature of MoS_2. The jump of thickness at edge of MoS_2 sheet is due to nanoscroll of several MoS_2 monolayers. From atomic force microscopy images the rms value of the surface roughness was found to be less than ~2.5 nm.

Raman spectra of MoS_2 monolayer vs. the gating voltage

Figure 2a and Fig. S1, SI show typical Raman spectra obtained from a CVD MoS_2 monolayer measured in our fabricated devices. Raman spectra were recorded with 632.8 nm laser excitation using a Witec confocal spectrometer (100x objective). They exhibit two characteristic peaks: one near 386.7 cm^{-1} and the other one near 403.4 cm^{-1}. The first one is attributed to an in-plane vibrational mode E^1_{2g}, and the second one is attributed to an out-of-plane vibrational mode A_{1g} (both modes are connected to the presence of MoS_2 monolayer). It is worth noting that the peak position of the E^1_{2g} mode was blue-shifted from 386.0 cm^{-1} (observed in mechanically exfoliated MoS_2[24]) to 386.7 cm^{-1}, while the peak position of the A_{1g} mode was also blue-shifted from 403.0 cm^{-1} to 403.4 cm^{-1} for the studied Au/Si_3N_4/MoS_2 structures. Analogous blue shifts of Raman peaks were observed in a hybrid system comprising MoS_2 and gold nanorods.[25] The separation $\Delta\nu$ between the E^1_{2g} and A_{1g} modes is ~17 cm^{-1}, which is close to the previously reported value for CVD-grown and mechanically exfoliated monolayer MoS_2.[24] The Raman data confirm the high

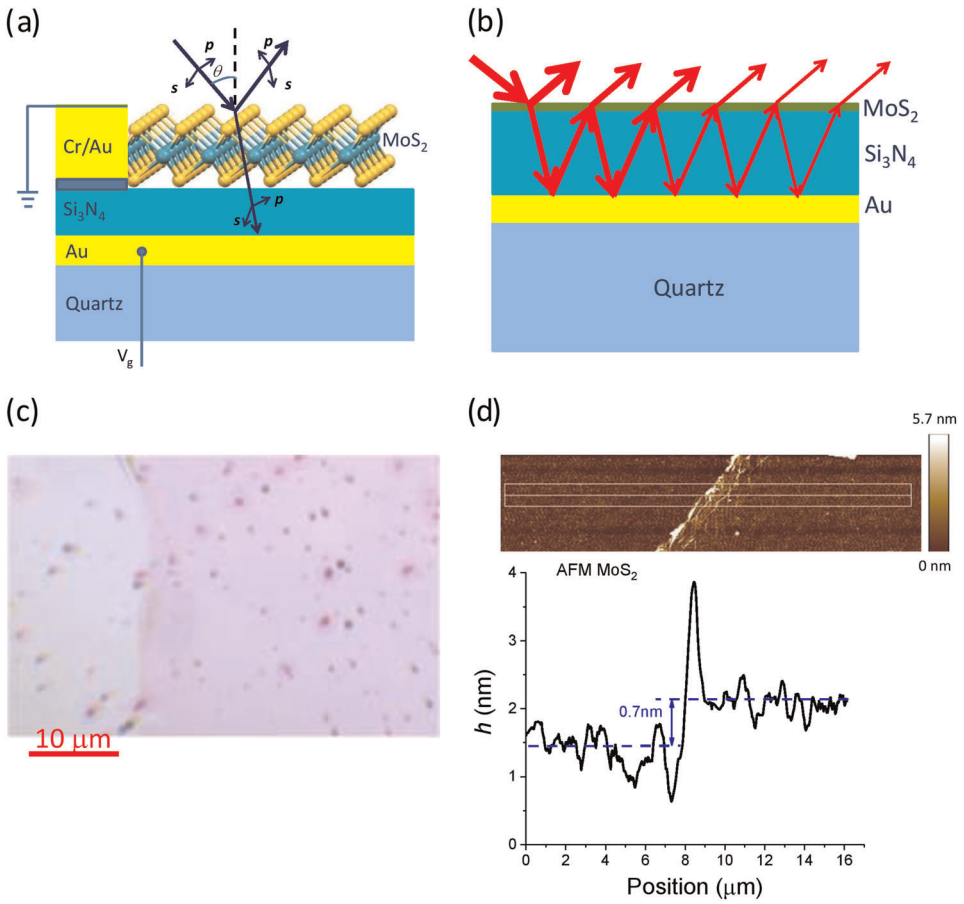

Fig. 1 Effect of interference on the electrical modulation of the reflectance in Au/Si_3N_4/MoS_2 hybrid waveguide nanostructure. **a** Schematic illustration of the device structure and principle of ellipsometric measurements. **b** The enhancement of the absorption in the MoS_2 monolayer due to multiple internal reflections at each interface of the Au/Si_3N_4/MoS_2 hybrid waveguide nanostructure. **c** Optical microscopy image of typical devices showing the top MoS_2 monolayer covering. **d** Contact-mode AFM of the device confirms monolayer nature of MoS_2

quality of the transferred MoS_2 on the Si_3N_4-based waveguide. Next, we performed complementary studies of MoS_2 monolayer Raman signals as a function of the gating voltage, see Fig. 2a. We found that the peak positions of E^1_{2g} and A_{1g} modes were largely unaffected by the V_g within the experimental error of $\pm 0.2\,cm^{-1}$ while Raman intensities of both E^1_{2g} and A_{1g} modes for $Au/Si_3N_4/MoS_2$ hybrid nanostructure changed significantly with the applied gate voltage. According to previous studies,[5] the intensity ratio of the Raman peaks could be used to explore exciton properties (bandgap renormalisation, damping factors, oscillator strengths associated with the excitons) of a MoS_2 monolayer. For example, the ratio of intensities of the E^1_{2g} and A_{1g} peaks (I_{E2g}/I_{A1g}) of MoS_2 could be used to identify the number of layers in MoS_2 (Fig. 2a and Fig. S1). The relative ratio I_{E2g}/I_{A1g} of the Raman bands of a MoS_2 monolayer as a function of V_g is shown in Fig. 2b. We can see that the intensity ratio I_{E2g}/I_{A1g} changes by ~30% with the gate voltage. In contrast, no significant change was observed in the relative ratio I_{E2g}/I_{A1g} at the same excitation conditions as a function of V_g for quartz/Si_3N_4/MoS_2 hybrid nanostructure (not shown here). This suggests that the intensity ratio I_{E2g}/I_{A1g} is changing due to the field-induced charge carrier density Δn in a MoS_2 monolayer. Injected carriers Δn mostly affect the optical properties of the MoS_2 monolayer due to the Coulomb scattering effect.[26,27]

It is interesting to note that while our measurements show a strong increase of Raman intensities for both the E^1_{2g} and A_{1g} modes with applied gating voltage they display no dependence of the Raman shifts on V_g for both modes. At the same time, it was demonstrated in ref. [28,29] that a gate-induced electron doping results in the shifts (up to $4\,cm^{-1}$) of the A_{1g} mode. Such behaviour was attributed to the occupation of the antibonding states in the conducting band of MoS_2 from the increased electron concentration.[28] The discrepancy between our data and those of refs. [28,29] is a mystery. One possible answer could lie in different excitation wavelengths at which Raman signals were measured. Our Raman spectra were recorded with 632.8 nm laser excitation which is in the resonance with excitation transitions. In contrast Raman data of MoS_2 monolayer were measured in ref. [28] with $\lambda_{exc} = 514.5$ nm and[29] with $\lambda_{exc} = 488$ nm which implies non-resonant Raman response. Note that the Raman spectra of CVD MoS_2 are affected by defects (usually an amount of defects in CVD MoS_2 monolayer is larger than that in mechanically exfoliated monolayer), and strain existing at the interface between the MoS_2 and Si_3N_4 layers, which depend on the lattice mismatch between above two nanostructures. Main difference between resonant and nonresonant excitation of Raman scattering is next: the resonance condition promotes the system to be excited into a bound exciton electronic states of MoS_2 monolayer. We can assume that the gate-dependent Raman intensity, shift and linewidth of MoS_2 monolayer are results of the combined effect of charge carrier density in the conducting band and exciton charges in the case of resonant-like excitation. The Raman signals of a MoS_2 monolayer (shown in Fig. 2 and Fig. S1), as well as its photoluminescence (Fig. S2), have revealed a strong dependence on an underlying optical structure due to substrate-related optical interference effects.[30]

Reflection at normal angle of incidence

At normal incidence, an application of V_g affects the reflectivity of the $Au/Si_3N_4/MoS_2$ hybrid nanostructure at wavelengths associated with the excitonic transitions.[7] Electric-field-dependent ratios of the reflection spectra $R(V_g)/R(V_g = 0\,V)$ are shown in Fig. 2c. We see that $R(V_g)/R(V_g = 0\,V)$ reflection spectra of the structure has a single local maximum at $\lambda \sim 665$ nm for positive values of V_g

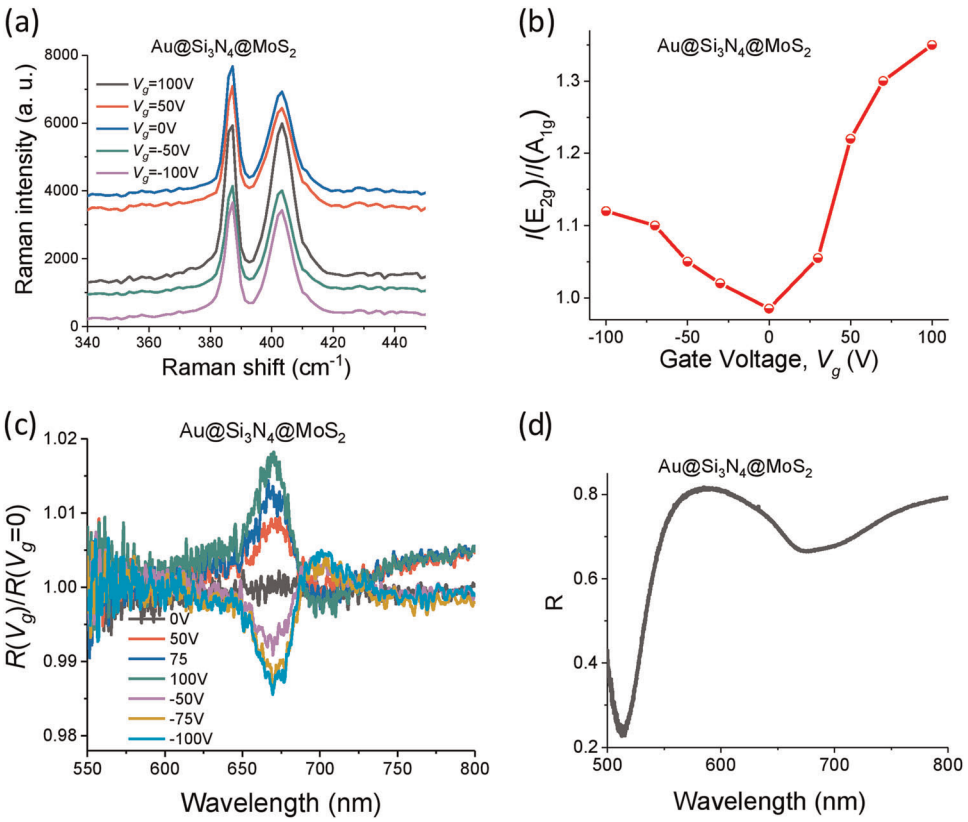

Fig. 2 Evolution of the vibration and optical spectra of the MoS_2 monolayer under gating voltage and changes of Raman spectra of monolayer MoS_2 at different gating voltage, V_g. **a** Gating tunability of vibration modes in monolayer MoS_2. **b** The measured Raman intensity ratio as a function of gating voltage, V_g. Reflection at normal angle of incidence. **c** Comparison of relative reflection spectra at normal incidence for different V_g. **d** The reflectivity of $Au/Si_3N_4/MoS_2$ hybrid waveguide nanostructure at normal incidence

and a minimum within the same spectral range for negative values of V_g. The amplitude of the $R(V_g)/R(V_g = 0\,\mathrm{V})$ features increase as the electrical field rises. At the same time, the change in reflection at $V_g = \pm 100$ V is relatively small and can be estimated as ~2%. The quality of Si_3N_4 film as insulating layer is quite good as the leakage (gate) current monotonically increases from 0.3 nA to 1 nA at room temperature when the gate voltage reaches 100 V. The reflection spectrum (shown in Fig. 2d) exhibits insertion loses closed to 70%. Spectral ellipsometric and FTIR measurements (Figs. S3 and S4, see SI) also confirm the high quality of CVD Si_3N_4 insulating-guiding layer.

Ellipsometry measurements

To characterise the field-effect tunability of the refractive index $(\tilde{n} = n + ik)$ of a MoS_2 monolayer, we measured the ellipsometric spectra of the monolayer as a function of gate voltages applied to a Au/Si_3N_4/MoS_2 hybrid nanostructure. The ellipsometric measurements (Fig. S5) were performed in the 240−1700 nm wavelength range with a variable angle spectroscopic ellipsometer (VASE, J.A. Woollam Co., Inc.). Data was collected at angles of incidence from 50° to 75° with a 5° angle interval. To model the measured ellipsometric spectra, we used a Fresnel multilayer model containing a quartz substrate, a Au layer, a Si_3N_4 dielectric, and a MoS_2 monolayer (0.7 nm thickness). The modelling was performed with the help of Woollam WVASE32 software, see SI. In our fitting procedure of ellipsometric parameters Ψ and Δ we used isotropic model and only the in-plane optical constants are derived because the reflectance change stronger for *s*-component of incident light (in plane of monolayer) and the roughness of substrate (Si_3N_4 deposited film) exceed the thickness of monolayer about 4 times. The bare quartz/Au/Si_3N_4 and quartz/Si_3N_4 structures were also measured and modelled using optical constants for Au and Si_3N_4 films extracted from separate ellipsometric measurements. The gate induced optical constant dependences for MoS_2 monolayer presented in Fig. 3a, b. We observed two prominent peaks in $n(\lambda)$ and $k(\lambda)$ spectra in the wavelength range 550–700 nm (Fig. 3a, b), the so-called A and B exciton bands which correspond to excitonic transitions between the valence band split by spin-orbit interaction and the conductance band.[7,31] A gate voltage dependent change of the charge carrier density may be mainly responsible for the variation of optical constants in vicinity of exciton bands (600–700 nm). It can be seen that a change of the polarity of the gate voltage leads to change the sign in deviation of optical constants Δn and Δk of MoS_2 monolayer respect to the $V_g = 0$ V. The extracted dielectric function, $\varepsilon(\omega) = (n + ik)^2$, of a CVD MoS_2 monolayer can be modelled by fitting with a multi-Lorentzian function[32]

$$\varepsilon(\omega) = 1 + \sum_{k=1}^{N} \frac{f_k}{E_k^2 - E^2 - iE\gamma_k}, \quad (1)$$

where f_k, E_k, and γ_k are the oscillator strength, the spectral resonance energy E_k, and the spectral width γ_k of the *k*-th oscillator, respectively. These values for the model parameters for a MoS_2 monolayer were determined by fitting Eq. (1) to the experimental data presented in Fig. 3a, b and S5. A good agreement between the extracted experimental dependences of the complex refractive index $(\tilde{n} = n + ik)$ and the analytical formula (1) were obtained for the f_k, E_k, and γ_k parameters presented in the (Table 1).

Furthermore, we demonstrate that the extracted real, *n*, and imaginary parts, *k*, of the refractive index in the range 600–700 nm decreases with the increasing gate voltage, V_g, which indicates suppression of the contributions from A and B excitonic transitions. With V_g increasing from 0 to 75 V, the absorption intensities $(\alpha = 4\pi k/\lambda)$ of both A and B excitons decrease significantly while their spectral positions are slightly red-shifted (Fig. S6). It is important to note that only the f_k and γ_k parameters for exciton A and B change significantly with the applied gate voltage. Figure 3 shows the dependence of optical constants as a function of V_g and results of fitting for oscillator strength f_k, and the spectral width γ_k in the case of negative and positive gating and strong changes of these parameters as a function of electron density n_e induced by the gate voltage. From Fig. 3 we conclude that the optical constants of a monolayer MoS_2 are gate-tunable in the spectral range from 580 to 750 nm. At the same time, $n(\lambda)$ and $k(\lambda)$ are V_g-independent outside the spectral range of MoS_2 excitons. Therefore, we are to expect optoelectronic modulation of the reflection from the studied structure in the spectral range of MoS_2 excitons.

It is worth noting that Fig. 3a, b reports the first observation (to the best of our knowledge) of an evolution of $n(\lambda)$ and $k(\lambda)$ spectra with a gating voltage for a MoS_2 monolayer *extracted from variable angle of incidence measurements of the ellipsometric parameters* Ψ and Δ. When V_g increases (from −100 to +75 V) the A and B exciton intensities become weaker and full widths at half maximum become larger, respectively. Gate-dependent absorption associated with the low-energy A exciton diminishes more rapidly than one of B exciton. When the V_g is varied from −100 to +75 V the exciton energy red-shifts slightly. It is interesting to note that the dependences for the real part of refractive index experience a blue-shifts as V_g increases. These dependences arise from the combined effects of Pauli blocking and many-body interactions.[33] The complex refractive index of a MoS_2 monolayer as a function of gate voltage in our study is consistent with pioneering experimental results of work,[34] in which the complex permittivity of monolayer MoS_2 was extracted from differential transmission and reflection spectra. In ref. [33] was shown that the exciton peak A can be split into two resonances in the case of low temperature measurements (10 K), where low-energy feature correspondent to negative trions while the other one associated with neutral A exciton.

Reflection at oblique angles of incidence

More prominent electro-optical modulation of reflection from our structures can be achieved at larger angles of incidence where light can couple to waveguide modes of the device leading to pronounced Fabry-Perot resonances. The reflection measurements of both *p*-polarised and *s*-polarised light in the spectral range of 240–1000 nm have been performed with a Woollam ellipsometer that has a focusing spot of about 50 μm. Figure 4a, b show reflectance of the Au/Si_3N_4/MoS_2 hybrid nanostructure for different states of polarised light as a function of angle of incidence (the thickness of Si_3N_4 layer was 390 nm). We see the excited resonant modes as reflection features for both polarisations. There are narrow interference minima for reflection of *s*-polarised light and pronounced maxima for reflection of *p*-polarised light observed in the range of 550–700 nm. For example, at zero gate voltage the reflection spectrum for *s*-polarised light (R_s) exhibits a pronounce and narrow minimum at λ ~625 nm for $\theta_{inc} = 80°$. Figure 5 shows the polarised reflectance of Au/Si_3N_4/MoS_2 hybrid nanostructure for different angles of incidence at $V_g = 0, \pm 100$ V as a function of the photon wavelength. Strong absorption is obtained for narrow spectral range for *s*-polarisation (Figs. 4 and 5) at larger incident angles (above 70°). The results in Fig. 5 demonstrate that the resonance of $R_s(\lambda)$ is shifted to longer wavelength as the incidence angle is decreased which leads to reducing of modulation effect. We would like to note that the change of the polarity of the gate voltage lead to change the sign of $R_s(\lambda)$ at resonance wavelength respect to $V_g = 0$ V for angles $\theta_{inc} < 75°$. When our device illuminated with *p*-polarised light, the modulated reflectance exhibits a small change (about 2–3%).

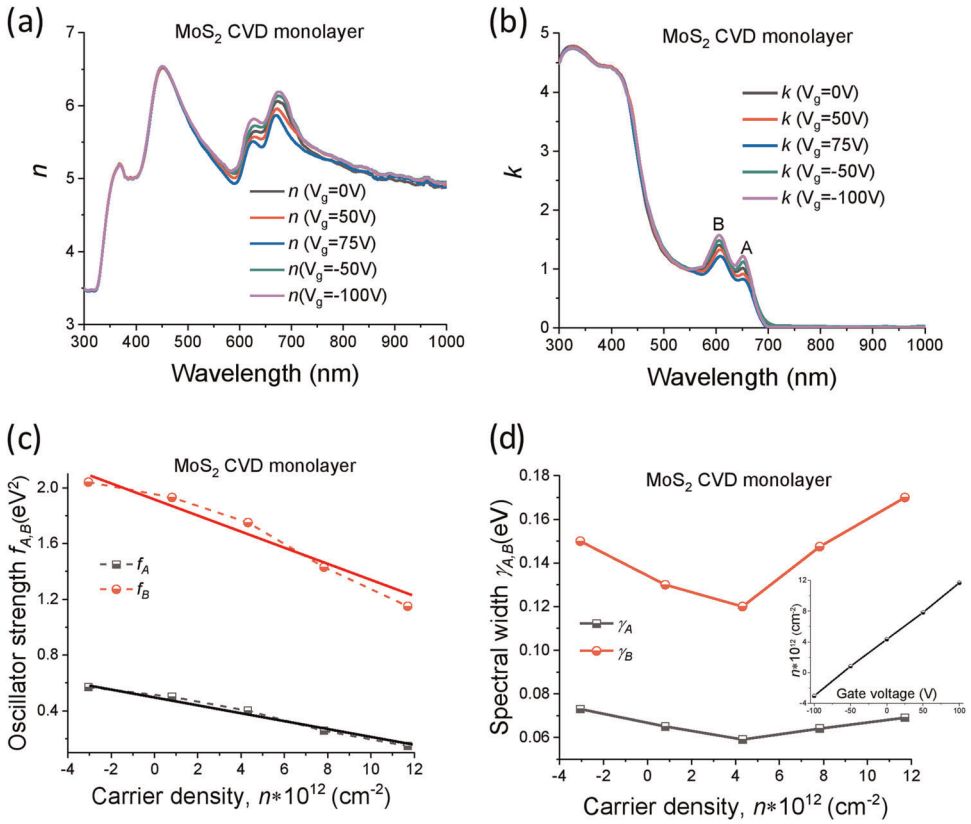

Fig. 3 Gate induced changes in the complex refractive index, $(\tilde{n} = n + ik)$ of MoS_2 monolayer extracted from ellipsometric measurements: the real part, n (**a**) and the imaginary part, k (**b**). Electrical tuning of the Lorentzian parameters for the complex refractive index of the CVD MoS_2 monolayer. **c** Oscillator strengths, $f_{A,B}$ and (**d**) Spectral width of A and B excitonic absorption bands, $\gamma_{A,B}$ as a function of density of injected charge carrier density, n_e. The solid lines in Fig. 3(c) show the linear fit to the data. Inset: the gate-dependent density of induced charge carriers

Table 1. Fitting parameters for the complex refractive index of the CVD MoS_2 monolayer as a function of gate voltage

k	MoS_2 monolayer					
	$V_g = 0$ V			$V_g = 75$ V (−100 V)		
	E_k (eV)	f_k(eV^2)	γ_k(eV)	E_k (eV)	f_k(eV^2)	γ_k(eV)
1(A)	1.89	0.4	0.059	1.89	0.15 (0.57)	0.068 (0.073)
2(B)	2.03	1.75	0.12	2.03	1.15 (2.03)	0.17 (0.15)
3	2.877	42.5	0.37	2.87	42.5	0.37
4	2.275	5.0	1.2	2.275	5.0	1.2
5	3.745	160	1.3	3.77	160	1.3

The refractive index is given by the multi-Lorentzian dispersion relation defined by Eq. (1). The oscillator strength f_k, the spectral resonance energy E_k, and the spectral width γ_k of the k-th oscillator are given in eV^2, eV, and eV, respectively

We found that interaction between light and a MoS_2 monolayer in our devices increased for larger angle of incidence resulting in larger electro-optical modulation. Figure 4c, d shows the changes of s-polarised reflectance $R(V_g)$ with gate voltage at the angle of incidence 80°. We can see that in the range of gate voltages between 0 and ±100 V, the absolute value of $R_s(V_g)$ is changing by more than 10%. The relative changes of reflectance $(R_s(V_g)/R_s(0))$ are much larger and reach 440%. This gives the modulation depth of 6 dB with insertion losses at the level of 15 dB. As was shown experimentally,[35,36] it is possible to achieve the modulator depths >15 dB for modulators based on graphene working in the infrared (~1500 nm). However, it is virtually impossible to extend the working range of graphene modulators to visible light. MoS_2 provides a nice alternative to graphene for visible light modulators. Indeed, in this work we have experimentally achieved the modulation depth of ~6 dB for visible light (red light ~630 nm) for simple electro-optical modulator based on MoS_2 monolayers. This modulation depth observed in our device is among the best for TMDs based modulators.[4–6,37] The changes observed in Fig. 4c, d are attributed to the V_g induced refractive index changes (Fig. 3a, b) in the MoS_2 monolayer combined with the optical resonant features of the device. (Indeed, the modulation at 80° light incidence happens in a narrow resonant band near 625 nm with a half width at half maximum of ~12 nm.) We also observed field-induced modulation for p-polarised light, albeit the changes in reflection were about 3–4 times smaller than those for s-polarised light, see Fig. 4c–f.

DISCUSSION

Carrier properties (concentration, mobility, etc.) of a MoS_2 monolayer are critical parameters that govern the electro-optical properties of 2D materials. Some of these properties can be deduced from Raman spectra of MoS_2 flakes.[28] Because electron-phonon coupling is stronger for out-of-plane vibration (A_{1g} mode) than for in-plane vibration (E^1_{2g} mode), the increased electron concentration in a MoS_2 monolayer produced by gating voltage causes the reduction and broadening of the A_{1g} mode, see Fig. 2a.

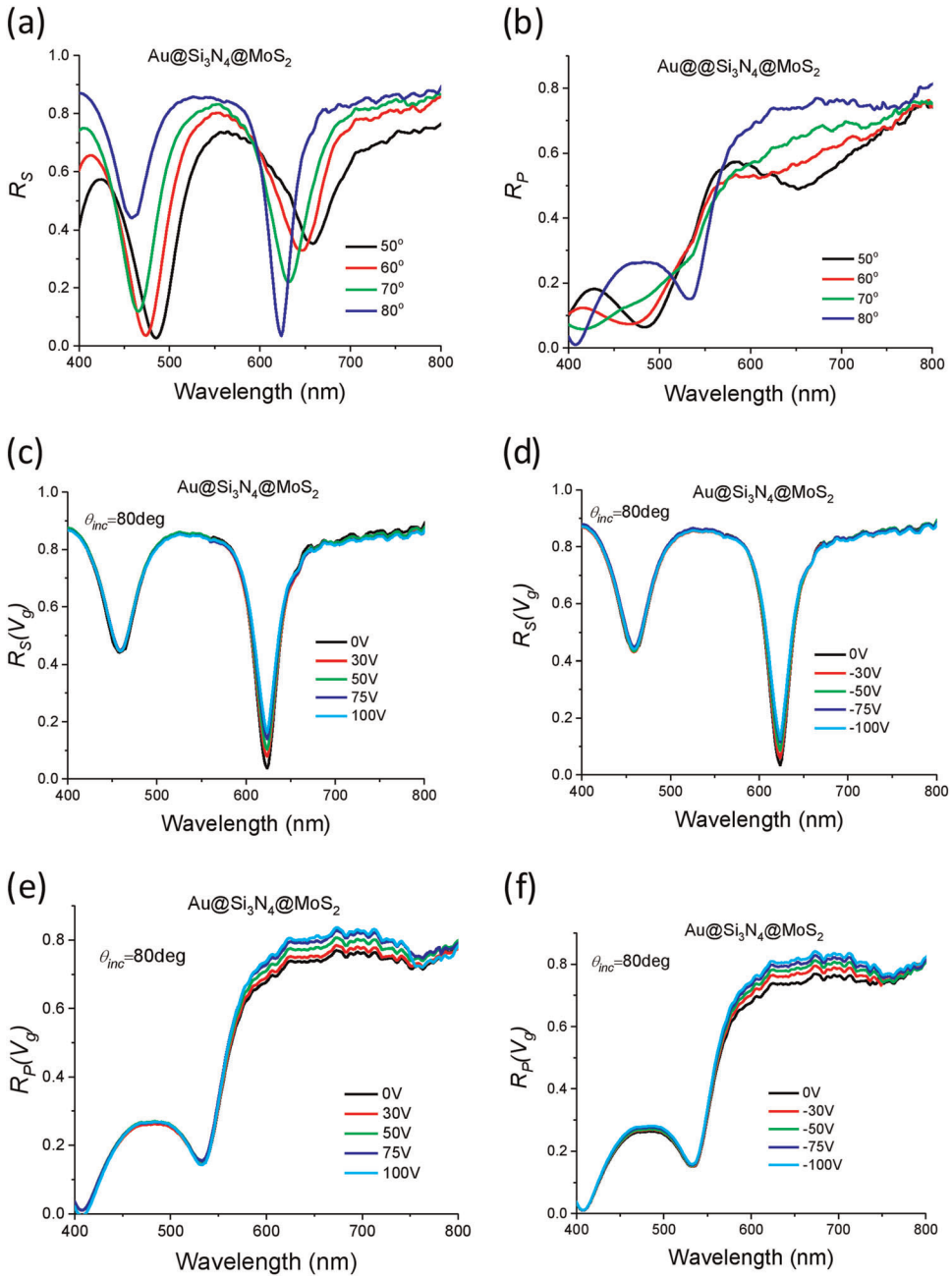

Fig. 4 Change in polarised reflectance for different gating voltages, V_g. **a**, **b** Reflection for *s*-polarised and *p*-polarised light in a broad spectral range from $Au/Si_3N_4/MoS_2$ hybrid waveguide nanostructure as a function of incident angle. **c**, **d** Change in *s*-polarised reflectance in the $Au/Si_3N_4/MoS_2$ hybrid nanostructure designed for this work in the spectral range of the A and B excitons. **e**, **f** Change in *p*-polarised reflectance in the $Au/Si_3N_4/MoS_2$ hybrid nanostructure designed for this work in the spectral range of the A and B excitons

The properties of the excitonic modes A and B which produce absorption peaks and gate-tunability of the refractive index (Fig. 3a, b) could be affected by substrate. Indeed, it is known that negative trions could be formed by neutral excitons after accepting an electron and the A mode can split onto two modes A^0 and A^-.[33,38] Hence, the broadening of the absorption spectra shown in Fig. 3b could be explained by superposition of contributions from neutral excitons and negative trions.[38] The dipole vibrations of electron-hole pairs (neutral excitons) and electron-electron-hole clusters (trions) are not necessarily coplanar which would allow light coupling to both *p*-polarisations and *s*-polarisations. In-plane dipole moments are prevalent in a MoS_2 monolayer due to symmetry, which was confirmed by study of momentum-resolved photoluminescence.[39] At the same time, out-of-plane dipole photo-luminescence emission is also present albeit much smaller than that of the in-plane dipole photo-luminescence. We observed narrow resonances for *s*-polarised reflection produced solely by in-plane dipoles while the response for *p*-polarised light was relatively weak at large angle of incidence (it contains mostly contributions from out-of-plane oriented dipoles), see Fig. 4a, b.

Next, we focus on the complex refractive index of a MoS_2 monolayer. Our measurement shows that the absorption is constant (gate-independent) away from the A and B excitonic bands. The dielectric constant (the refractive index) of the TMDs monolayer can be modelled by an oscillator multi-Lorentzian model which takes into account contributions from excitons.[32,40]

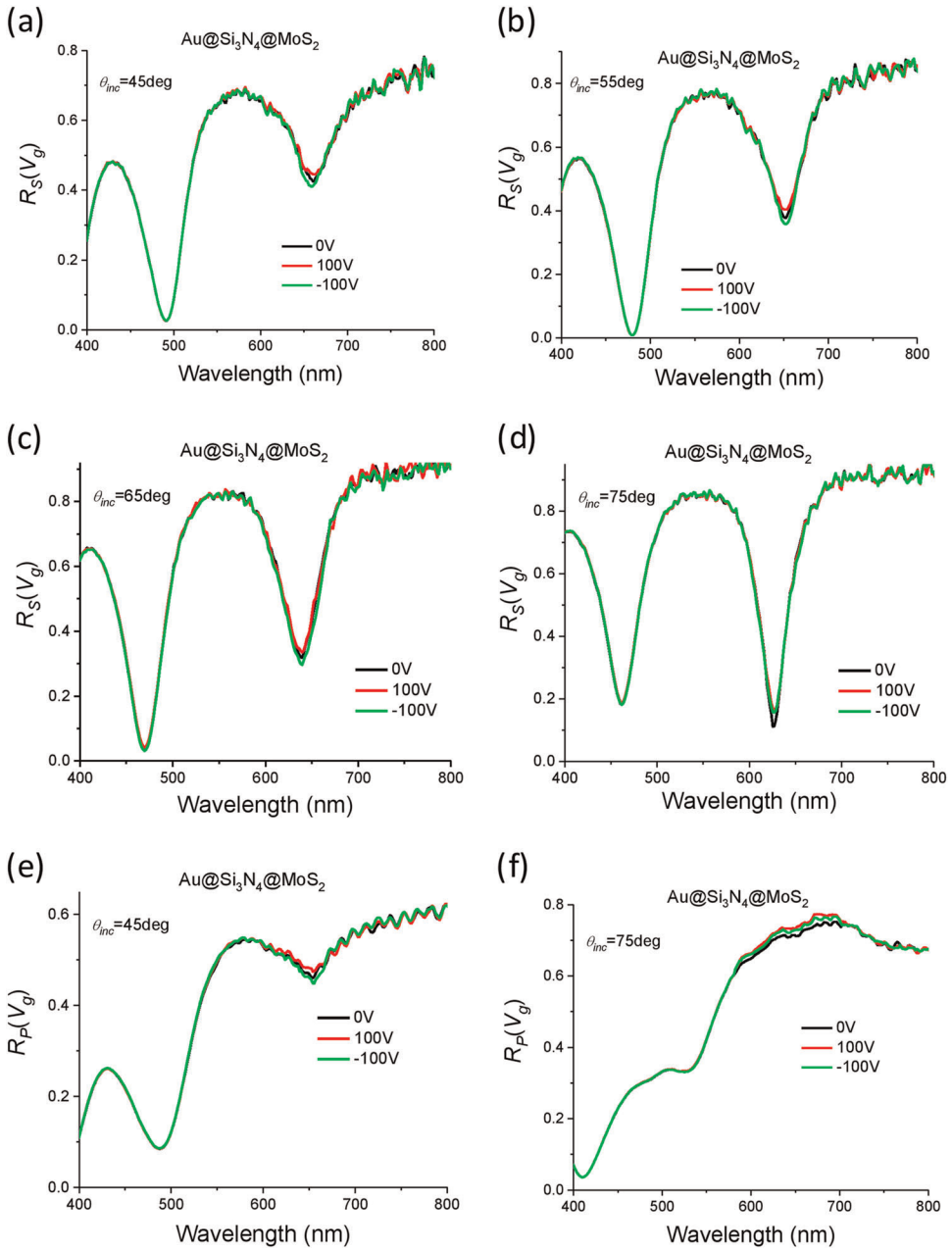

Fig. 5 The polarised reflection spectra as a function of incident angle (from 45° to 75°) and polarisation states (*p*-polarisation and *s*-polarisation). **a**-**d** Change in *s*-polarised reflectance in the $Au/Si_3N_4/MoS_2$ hybrid nanostructure in the spectral range of the A and B excitons for 45°, 55°, 65° and 75°. **e**, **f** Change in *p*-polarised reflectance in the $Au/Si_3N_4/MoS_2$ hybrid nanostructure in the spectral range of the A and B excitons for 45° and 75°

The change in absorption and electro-optical modulation arise when oscillator constants f_k, E_k, and γ_k (f_k, E_k, and γ_k are the oscillator strength, the resonance energy E_k, and the width γ_k of the *k*-the oscillator, respectively) are affected by constant electrical field. The fitting results (Fig. S6) show that only the oscillator strengths and widths for the A and B excitonic transitions exhibit significant variations under external electrical gating (Table 1). The excitonic transition energies E(A) and E(B) do not significantly change with V_g. This is in good agreement with theory[41] which predicts a cancellation of screening effects on single-particle band gap renormalisation and exciton binding energy. The observed changes in the refractive index are due to the decreasing of the oscillator strength $f_{A,B}$ and increasing the spectral width $\gamma_{A,B}$ under V_g (Table 1). In the measured gate voltage range $0 < V_g < 75$ V, the expected change in carrier density due to the electrical field effect can be estimated as $n_e = (\varepsilon_0 \varepsilon_{st} V_g)/(de)$ (where ε_0 is the permittivity of free space, ε_{st} is the static dielectric constant for Si_3N_4 film extracted from FTIR measurement (see, SI), *d* is the thickness of Si_3N_4 insulating film, and *e* is the electron charge). Consequently, the V_g induces change in *n*, causes a broadening of the spectral width of A and B excitonic absorption bands $\gamma_{A,B}$ and decreasing of the oscillator strengths, $f_{A,B}$, which are presented in Fig. 3c, d. The effective concentration of electron in the MoS_2 surface for $V_g = 0$ was also estimated: $n_0 = 2(2\pi m_0 kT/h^2)^{3/2} = 4.32 \times 10^{12}$ cm^{-2} ($m_0 = 0.5m_e$ is the effective electron mass for MoS_2 bulk, *k* is the Boltzmann's constant, *T* is the temperature set at 300 K, and *h* is Planck's constant).

We suggest a possible mechanism for gate voltage dependent absorption in a MoS_2 monolayer in the vicinity of A and B exciton —the Pauli blocking effect.[42] In the Pauli blocking effect (phase-space filling) a carrier density increase makes part of the phase space unavailable for exciton formation due to the Pauli exclusion principle.[42] This effect can be described with the help of a multiexciton Wannier formalism.[43,44] (The Wannier exciton theory should be applicable in our case because the effective Bohr radius of an exciton $a_B = \hbar^2\varepsilon_{st}/(\mu e^2)$, where $\mu = 0.195m_e$ is the *e-h* reduced mass in unit of electron mass, and $\varepsilon_{st} = 3.43$ is the dielectric constant of the monolayer; this value is around 0.93 nm for MoS_2 monolayer which is larger than the in-plane lattice constant[43,44]). The theory is quite elaborate and suggests that for a MoS_2 monolayer the excitons and conduction electrons should occupy different regions of the phase space. This causes a reduction in the exciton oscillator strength with induced electron density which can be roughly described as

$$f_{A,B} = f^0_{A,B}(1 - n/n_{eff}) \approx f^0_{A,B}\left(1 - n \cdot \pi a_B^2\right). \quad (2)$$

To check this dependence, we have linear fitted the extracted oscillator strengths as a function of the induced electron density, see Fig. 3c. Using (2), we can evaluate an effective Bohr radius of an exciton from the linear fit parameters. The linear fit gives n_{eff} to be 1.6×10^{13} cm^{-2} and 2.6×10^{13} cm^{-2} and a_B to be 1.4 nm and 1.1 nm for A and B excitons, respectively. For the realistic case in which the MoS_2 monolayer locates between air (with a dielectric permittivity ε (air) = 1) and a dielectric medium Si_3N_4 (with a dielectric permittivity $\varepsilon_{st}(Si_3N_4) = 8.5$ evaluated from FTIR measurement, see SI, Eq(S1)) the dielectric constant can be calculated in the superpositional approximation: ε_{st}=[ε(air) + $\varepsilon_{st}(Si_3N_4)$]/2.[45] Using values of electron, $m_e/m_0 = 0.35$ and hole, $m_h/m_0 = 0.428$ effective masses in units of the bare electron masses, m_0[45] and the average of the $\varepsilon_{st} = 4.75$, we can estimate the exciton Bohr radius, $a_B^* \approx$ 1.3 nm. This theoretical value[45] is close to an effective Bohr radius of MoS_2 excitons evaluated from ellipsometric measurements.

Another contribution to decreasing of $f_{A,B}$ could come from changes in the exciton orbital wave function due to modification of *e-h* interaction induced by the presence of other *e-h* pairs.[42,44] This reduces the probability of finding an electron near a hole and also yields a contribution to the oscillator strength $f_{A,B}$. In addition to the change in $f_{A,B}$, broadening of the exciton bands (the spectral widths $\gamma_{A,B}$) could be observed after application of V_g. The broadening has collisional nature being governed by the Coulomb scattering effect, carrier density, and kinetic energy of the bonding *e-h* pairs and the individual charges.[42]

The changes in reflectance (R) can be associated with absorbance due to the energy conservation law. Indeed, the frequency-dependent absorption A of an optical structure can be calculated as $A = 1 - R - T$, where T is the total transmittance. For the studied Au/Si_3N_4/MoS_2 hybrid nanostructure, the Au layer is thick (~65 nm) so that transmittance of the structure is negligible. Hence, according to the Kirchhoff's law, the absorbance can be found as $A = 1 - R$. Therefore, changes in the refractive index of a MoS_2 monolayer induced by the electric field effect modify both reflectance of and absorbance of the structure. (It is worth noting that light absorption happens mostly within the top MoS_2 monolayer.) The appearance of multiple peaks in light absorbance of the hybrid nanostructure shown in Figs. 4 and 5 is connected with Fabry–Perot resonances produced in the studied waveguide-based heterostructure[46] as explained in the modelling section and SI. At large angles of incidence, the reflection coefficients become large which increases the quality and depths of the Fabry–Perot resonances. As a result, photons become trapped for a longer time in the heterostructure and experience more bounces from the MoS_2 layer which leads to the enhanced absorption of the structure. The large enhancement of absorption can also be explained in terms of optical interference produced by multi-reflection and multi-refraction at the interfaces. The interference can enhance the local electrical fields around the MoS_2 monolayer and hence increase the light modulation produced by changes in the excitonic properties induced by the electric field effect (gating voltage). The concentration of electrical field inside of the Si_3N_4 layer significantly depends on how close incident angle θ is to θ_c (where the θ_c is the angle of TIR at Si_3N_4/Air interface: $\theta_c = \arcsin(1/n_d) \sim 29°$ at $\lambda \sim 625$ nm). If the angle of incidence θ inside of Si_3N_4/MoS_2 nanostructure larger than θ_c, no beam propagated outside of Si_3N_4. Due to high refraction index of MoS_2 monolayer (Fig. 3) the density of trapping light in dielectric cavity becomes higher. Probing light can be confined in the top Si_3N_4/MoS_2 layers by internal reflection at MoS_2/Si_3N_4 and MoS_2/Air interfaces. Thus indeed MoS_2/Si_3N_4/Au structure can act like a waveguide and we see multiple dips in the reflectance spectra.

The enhancement of absorbance observed in the measurements can be qualitatively reproduced by transfer matrix calculations and is associated with excitation of Fabry–Perot resonances in the multilayer structure[47,48] (see Supplementary Information for details). At first stage the light absorption of MoS_2 in the spectral region of excitons was optimised for light incidence with respect to thickness of dielectric Si_3N_4 layer. Figure S7 shows the calculated *s*-polarised reflection of MoS_2/Si_3N_4/Au nanostructure as a function of the incident wavelength and the thickness of the dielectric Si_3N_4 layer, suggesting that the optimised Si_3N_4 thickness is in the range of 390–415 nm. It is also evident that the linewidth of the resonance changes by varying Si_3N_4 layer thickness. Our calculation also confirms that for an optimised Au/Si_3N_4/MoS_2 hybrid waveguide nanostructure the absorption enhancement in the spectral range of exciton bands of MoS_2 is strong and modulation of reflectance induced by external electrical field produced by gating voltage V_g is large (Fig. 6). Calculated values for *p*-polarised and *s*-polarised reflectance corresponding to our experimental conditions are shown in Fig. 6. A good agreement between experiment and calculations is observed for both polarisations. Note that the slight difference between experimental and theoretical dependences exists due to surface roughness and impurities on top of sample after MoS_2 transferring (see Inset Fig. 6a). The modelling shows that the multi-pass light interaction introduced by interference produces enhanced excitonic absorption in a 2D single layer. The modelling also confirms that the absorbance and reflectance of our structure can be indeed electrically tuned by 10–15% due to an injection of charge carriers into a MoS_2 monolayer resulting in refractive index modulation shown in Fig. 3b.

In summary, we have demonstrated the optical electric field effect on a MoS_2 monolayer combined with a dielectric Si_3N_4 waveguide layer placed on a gold sublayer. The light modulation due to an applied gate voltage was observed near excitonic bands of a MoS_2 monolayer. Using spectroscopic ellipsometry, we have extracted the dependence of the complex refractive index of a MoS_2 monolayer as a function of gate voltage (applied electric field). We have shown that the light modulation can be significantly enhanced by utilising Fabry–Perot resonances observed in the demonstrated hybrid nanostructures at large angles of incidence. The enhancement of light modulation is due to interference effects observed in the studied structure. We found that a simple Fresnel theory provides a good fit to the experimental data and allows one to model light modulation in the studied structure with help from the gate-dependent MoS_2 refractive index elucidated in our work. In contrast to optoelectronic devices based on other 2D materials (including graphene), the fabricated devices showed excellent durability and survived all the measurements for a period of more than one year (they are still alive). The fabricated low-cost waveguide nanostructure with a MoS_2 monolayer showed a large modulation range of ~6 dB for red light. This approach can find realistic

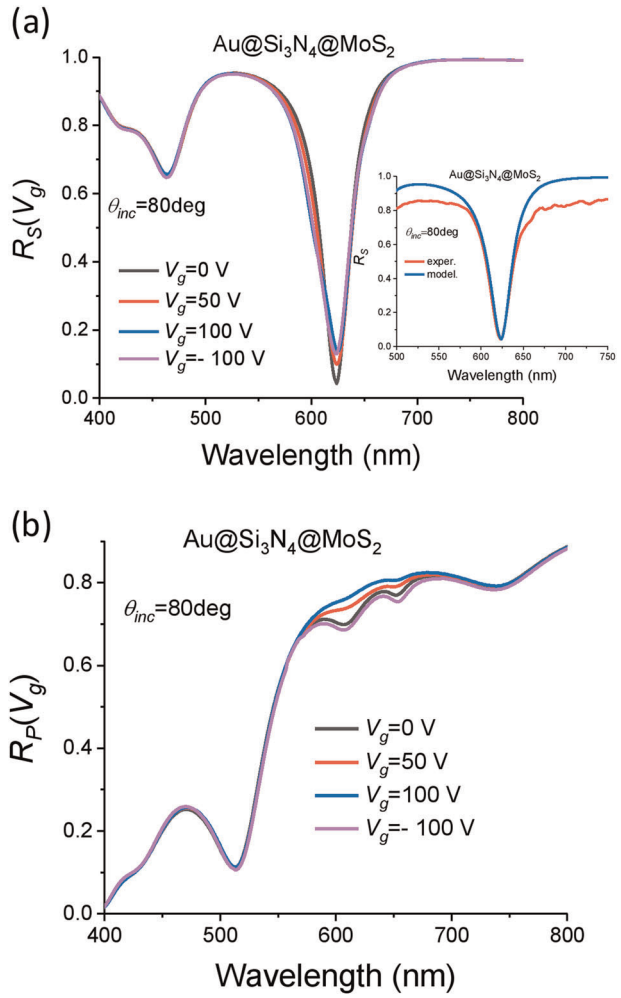

Fig. 6 Numerical simulations of the changes in *s*-polarised (**a**) and *p*-polarised (**b**) reflectance at gating voltages, V_g using the interference effect and electrical tunability of the refractive index of monolayer MoS_2. Inset: experimental and modelled *s*-polarised reflectance of the $Au/Si_3N_4/MoS_2$ hybrid waveguide nanostructure at $V_g = 0$

applications in designing optical modulators for the visible region of the spectrum.

METHODS

Fabrication of devices

Samples were fabricated using electron beam deposition, chemical vapour deposition, etching procedure and 2D material transfer. First, a 3 nm-thick Cr adhesion layer and 65 nm Au film were deposited on top of a 1 mm-thick quartz substrate using electron beam evaporation. Second, a Si_3N_4 waveguide layer was grown by chemical vapour deposition (CVD) to cover the Au film. Third, a monolayer of MoS_2 (grown by the CVD method on Si/SiO_2 substrate and acquired from 2D Semiconductors) was spin coated with a poly(methyl methacrylate) (PMMA) resist. Then, the $PMMA/MoS_2/SiO_2/Si$ stacks were set onto the scotch type with a window and floated in KOH solution until complete Si/SiO_2 etching which happened within a few hours. Next, the $PMMA/MoS_2$ films on the scotch type were rinsed with DI water and fished for transfer procedure. Fourth, the resulting monolayer of MoS_2 was transferred on top of quartz/Au/Si_3N_4 structure.

Measurement and characterisation

Raman and photoluminescence (PL) spectra of the CVD grown MoS_2 monolayer was recorded with a Witec confocal Raman spectrometer at the excitation wavelengths of 514 nm and 632.8 nm. Fourier Transform Infra-Red (FTIR) spectroscopy was performed with the help of a Bruker Vertex 80 system and a Hyperion 3000 microscope. A variety of sources and detectors, combined with aluminium coated reflective optics enable this system to be used from visible to mid-IR wavelengths.

We also performed an accurate determination of the complex refractive index and thickness of a MoS_2 monolayer using a variable angle Woollam M2000F focused-beam spectroscopic ellipsometer. The spot size on the sample was approximately 30×80 µm at ~70–80° angles of incidence. Ellipsometry measures two parameters, Ψ (reflection) and Δ (phase), which are related to the complex amplitude reflectance ratio: $\tan(\Psi)\exp(i\Delta) = r_p/r_s$, where r_p and r_s are the amplitude reflection coefficients for *p*-polarised and *s*-polarised light. In addition to ellipsometric parameters Ψ and Δ, the ellipsometer allowed us to separately measure R_p and R_s, the intensity reflections for *p*-polarised and *s*-polarised light, respectively, at various angles of incidence with respect to the total light intensity.

DATA AVAILABILITY

The data that support the findings of this study are available from the corresponding author on reasonable request.

ACKNOWLEDGEMENTS

We thank V. Falko and T. Wehling for sharing their extensive knowledge connected to exciton physics. A.N.G. acknowledges the support from the EU Graphene Flagship and SONY research grant agreement. We also acknowledge support from EPSRC Grant EP/L01548X/1.

AUTHOR CONTRIBUTIONS

A.V.G. and V.G.K. conceived the experiment, V.G.K. and G.H.A. fabricated the samples, V.G.K., T.Y., F.W. and S.I., carried out the electro-optical and optical measurements, V.G.K., T.Y. and A.V.G. theoretically modelled the electro-optical modulator based on 2D material, A.V.G. and V.G.K. analysed the data and prepared the paper. All authors discussed the results.

ADDITIONAL INFORMATION

Supplementary Information accompanies the paper on the *npj 2D Materials and Applications* website (https://doi.org/10.1038/s41699-019-0119-1).

Competing interests: The authors declare no competing interests.

Publisher's note Springer Nature remains neutral with regard to jurisdictional claims in published maps and institutional affiliations.

REFERENCES

1. Reed, G. T., Mashanovich, G., Gardes, F. Y. & Thomson, D. J. Silicon optical modulators. *Nat. Photon.* **4**, 518–526 (2010).
2. Xia, V., Wang, H., Xiao, D., Dubey, M. & Ramasubramaniam, A. Two-dimensional material nanophotonics. *Nat. Photon.* **8**, 899–907 (2014).
3. Mak, K. & Shan, J. Photonics and optoelectronics of 2D semiconductor transition metal dichalcogenides. *Nat. Photon.* **10**, 216–226 (2016).
4. Sun, Z., Martinez, A. & Wang, F. Optical modulators with 2D layered materials. *Nat. Photon.* **10**, 227–238 (2016).
5. Yu, Y. et al. Giant gating tunability of optical refractive index in transition metal dichalcogenide monolayers. *Nano Lett.* **17**, 3613–3618 (2017).
6. Vella, D. et al. Unconventional electroabsorption in monolayer MoS_2. *2D Mater.* **4**, 021005 (2017).
7. Mak, K. F., Lee, C., Hone, J., Shan, J. & Heinz, T. E. Atomically thin MoS_2: a new direct-gap semiconductor. *Phys. Rev. Lett.* **105**, 136805 (2010).
8. Radisavljevic, B., Radenovic, A., Brivio, J., Giacometti, V. & Kis, A. Single-layer MoS_2 transistors. *Nat. Nanotechnol.* **6**, 147–150 (2011).
9. Cui, X. et al. Multi-terminal transport measurements of MoS_2 using a van der Waals heterostructure device platform. *Nat. Nanotechnol.* **10**, 534–540 (2015).
10. Novoselov, K., Mishchenko, A., Carvalho, A. & Neto, A. C. 2D Materials and van der Waals heterostructures. *Science* **353**, 9439–9450 (2016).
11. Liu, F., Zhou, J., Zhu, C. & Liu, Z. Electric field effect in two-dimensional transition metal dichalcogenides. *Adv. Funct. Mater.* **27**, 1602404 (2017).
12. Geim, A. K. & Grigorieva, I. V. Van der Waals heterostructures. *Nature* **499**, 419–425 (2013).

13. Wang, Q. H., Kalantar-Zaden, K., Kis, A., Coleman, J. N. & Strano, M. A. Electronics and optoelectronics of two-dimensional transition metal dichalcogenides. *Nat. Nanotechnol.* **7**, 699–712 (2012).
14. Kravets, V. G. et al. Plasmon-induced nanoscale quantised conductance filaments. *Sci. Rep.* **7**, 2878 (2017).
15. Bernardi, M., Palummo, M. & Grossman, J. C. Extraordinary sunlight absorption and one nanometer thick photovoltaics using two-dimensional monolayer materials. *Nano Lett.* **13**, 3664–3670 (2013).
16. Kravets, V. G., Neubeck, S., Grigorenko, A. N. & Kravets, A. F. Plasmonic blackbody: strong absorption of light by metal nanoparticles embedded in dielectric matrix. *Phys. Rev. B* **81**, 165401 (2010).
17. Kravets, V. G. & Grigorenko, A. N. Retinal light trapping in textured photovoltaic cells. *Appl. Phys. Lett.* **97**, 143701 (2010).
18. Janisch, C. et al. MoS_2 monolayers on nanocavities: enhancement in light-matter interaction. *2D Mater.* **3**, 025017 (2016).
19. Lee, Y.-Ch, Tseng, Y.-Ch & Chen, H.-L. Single type of nanocavity structure enhances light outcouplings from various two-dimensional materials by over 100-fold. *ACS Photon.* **4**, 93–1005 (2017).
20. Sobbani, A. et al. Enhancing the photocurrent and photoluminescence of single crystal monolayer MoS_2 with resonant plasmonic nanoshells. *Appl. Phys. Lett.* **104**, 031112 (2014).
21. Rodriguez, F. J., Aznakayeva, D. E., Marshall, O. P., Kravets, V. G. & Grigorenko, A. N. Solid-state electrolyte-gated graphene in optical modulators. *Advan. Mater.* **29**, 1606372 (2017).
22. Moss, D. J., Morandotti, R., Gaeta, A. L. & Lipson, M. New CMOS-Compatible platforms based on silicon nitride and Hydex for nonlinear optics. *Nat. Photon.* **7**, 597–607 (2013).
23. Thomas, P. A., Auton, G. H., Kundys, D., Grigorenko, A. N. & Kravets, V. G. Strong coupling of diffraction coupled plasmons and optical waveguide modes in gold stripe-dielectric nanostructures at telecom wavelengths. *Sci. Rep.* **7**, 45196 (2017).
24. Najmaei, S. et al. Vapour phase growth and grain boundary structure of molybdenum disulphide atomic layers. *Nat. Mater.* **12**, 754–759 (2013).
25. Shi, Y. et al. Hot electron of Au nanorods activates the electrocatalysis of hydrogen evolution on MoS_2 nanosheets. *J. Am. Chem. Soc.* **137**, 7365–7370 (2015).
26. Chernikov, A. et al. Exciton binding energy and nonhydrogenic Rydberg series in monolayer WS_2. *Phys. Rev. Lett.* **113**, 076802 (2014).
27. Ugeda, M. M. et al. Giant bandgap renormalization and excitonic effects in a monolayer transition metal dichalcogenide semiconductor. *Nat. Mater.* **13**, 1091–1095 (2014).
28. Chakraborty, B. et al. Symmetry-dependent phonon renormalization in monolayer Mo_s2 transistor. *Phys. Rev. B* **85**, 161403(R) (2012).
29. Miller, B., Parzinger, E., Vernickel, A., Holleitner, A. W. & Wurstbauer, U. Photogating of mono- and few-layer MoS_2. *Appl. Phys. Lett.* **106**, 122103 (2015).
30. Sun, Y., Wang, R. & Liu, K. Substrate induced changes in atomically 2-Dimensional semiconductors: Fundamentals, engineering, and applications. *Appl. Phys. Rev.* **4**, 011301 (2017).
31. Splendiani, A. et al. Emerging photoluminescence in monolayer MoS_2. *Nano Lett.* **10**, 1271–1275 (2010).
32. Wooten, F. *Optical Properties of Solids*. (Academic Press, New York and London, 1972).
33. Mak, K. F. et al. Tightly bound trions in monolayer MoS_2. *Nat. Mater.* **12**, 207–211 (2013).
34. Mukherjee, B. et al. Complex electrical permittivity of the monolayer molybdenum disulphide (MoS_2) in UV and visible. *Opt. Mater. Express* **5**, 447–455 (2015).
35. Phare, C. T., Lee, Y.-H. D., Cardenas, J. & Lipson, M. Graphene electro-optic modulator with 30 GHz bandwidth. *Nat. Photon.* **9**, 511–514 (2015).
36. Mohsin, M. et al. Graphene based low insertion loss electro-absorption modulator on SOI waveguide. *Opt. Express* **22**, 15292–15297 (2014).
37. Li, B. et al. Single-nanoparticle plasmonic electro-optic modulator based on MoS_2 monolayers. *ACS Nano* **11**, 9720–9727 (2017).
38. Li, Y. et al. Photoluminescence of monolayer MoS_2 on $LaAlO_3$ and $SrTiO_3$ substrates. *Nanoscale* **6**, 15248–15254 (2014).
39. Schuller, J. A. et al. Orientation of luminescent excitons in layered nanomaterials. *Nat. Nanotechnol.* **8**, 271–276 (2013).
40. Li, Y. et al. Measurement of the optical dielectric function of monolayer transition-metal dichalcogenides: MoS_2, $MoSe_2$, WS_2, and WSe_2. *Phys. Rev. B* **90**, 205422 (2014).
41. Steinhoff, V., Rösner, M., Jahnke, F., Wehling, T. O. & Gies, C. Influence of excited carriers on the optical and electronic properties of MoS_2. *Nano Lett.* **14**, 3743–3748 (2014).
42. Schmitt-Rink, S., Chemla, D. S. & Miller, D. A. B. Theory of transient excitonic optical nonlinearities in semiconductor quantum-well structures. *Phys. Rev. B* **32**, 6601–6609 (1985).
43. Cheiwchanchamnangij, T. & Lambrecht, W. R. L. Quasiparticle band structure calculation of monolayer, bilayer, and bulk MoS_2. *Phys. Rev. B* **85**, 205302 (2012).
44. Lefebvre, P., Christol, P. & Mathieu, H. Confined excitons in semiconductors: correlation between binding energy and spectral absorption shape. *Phys. Rev. B* **52**, 5756–5759 (1995).
45. Mostaani, E. et al. Diffusion quantum Monte Carlo study of excitonic complexes in two-dimensional transition-metal dichalcogenides. *Phys. Rev. B* **96**, 075431 (2017).
46. Yeh, P. *Optical Waves in Layered Media*. (Wiley, New York, 1988).
47. Yariv, A. & Yeh, P. *Optical Waves in Crystal Propagation and Control of Laser Radiation*. (John Wiley and Sons, Inc., New York, 1983).
48. Born, M. & Wolf, E. *Principles of Optics* pp. 704 (Cambridge University Press, New York, 1999).

Open Access This article is licensed under a Creative Commons Attribution 4.0 International License, which permits use, sharing, adaptation, distribution and reproduction in any medium or format, as long as you give appropriate credit to the original author(s) and the source, provide a link to the Creative Commons license, and indicate if changes were made. The images or other third party material in this article are included in the article's Creative Commons license, unless indicated otherwise in a credit line to the material. If material is not included in the article's Creative Commons license and your intended use is not permitted by statutory regulation or exceeds the permitted use, you will need to obtain permission directly from the copyright holder. To view a copy of this license, visit http://creativecommons.org/licenses/by/4.0/.

© The Author(s) 2019